We continue by calculating $C(\mathbf{q},\omega)$, which is

$$C=\lim_{\mathbf{q},\omega\to 0}\frac{4\pi}{V_A}\left\{\sum_{\kappa,\kappa'}\mathcal{K}_{\kappa'\kappa}{}^{*}(\mathbf{q},\omega)\int\frac{d^3k}{(2\pi)^3}n_{\mathbf{k}}B_{\mathbf{q}}(-\kappa',\mathbf{k})\times\sum_n Z_n\exp(-i\kappa\cdot\mathbf{x}_n)\,|\,\mathbf{u}_n\cdot[[\kappa+\mathbf{q}]]\,|^2-\sum_{\substack{n,n'\\ \kappa}}Z_nZ_{n'}\exp(-i\kappa\cdot\mathbf{x}_{nn'})\,|\,\mathbf{u}_n\cdot[[\kappa+\mathbf{q}]]\,|^2\right\}.$$

With the help of Eq. (17), this can be rewritten as

$$C=-\lim_{\mathbf{q},\omega\to 0}\frac{4\pi}{V_A}\sum_{n,n'}Z_nZ_{n'}\sum_{\kappa,\kappa'}\exp[i(\kappa'\cdot\mathbf{x}_{n'}-\kappa\cdot\mathbf{x}_n)]\times S_{\kappa'\kappa}(\mathbf{q},\omega)\,(\mathbf{u}_n\cdot[[\mathbf{q}+\kappa]])\,(\mathbf{u}_n{}^{*}\cdot[[\mathbf{q}+\kappa']]),$$

so that we obtain Eq. (18) of the main text, and $\omega^2\to 0$ in the $\mathbf{q}\to 0$ limit for those modes (i.e., the acoustic modes) for which $\mathbf{u}_n$ becomes independent of $n$ in this limit.

PHYSICAL REVIEW VOLUME 175, NUMBER 3 15 NOVEMBER 1968

# Long-Wavelength Optical Lattice Vibrations in Mixed $KMgF_3$-$KNiF_3$ Crystals

A. S. Barker, Jr., J. A. Ditzenberger, and H. J. Guggenheim
*Bell Telephone Laboratories, Murray Hill, New Jersey 07974*

(Received 1 July 1968)

Infrared reflection and transmission data are analyzed to give the transverse and longitudinal phonons in mixed $KNiF_3$-$KMgF_3$ crystals for seven concentrations ranging from 0 to 100% Ni. Both one- and two-mode behavior are observed. A point-ion model is developed patterned on earlier work on simpler mixed-crystal systems. The model assumes randomly distributed impurity ions and nearest-neighbor forces. The model gives good agreement with the observed mode frequencies, and in particular it fits the observed splitting of one of the reststrahlen bands at intermediate compositions.

## I. INTRODUCTION

WELL-DEFINED infrared- and Raman-active phonon modes have been seen in several mixed-crystal systems of the type $A_yB_{1-y}$.[1-3] Near the ends of the composition range of a mixed crystal one ion can be viewed as an impurity and connections can be made with the theories of local modes and impurity resonance modes,[1] but for intermediate compositions no first-principles theories exist. The extra degrees of freedom resulting from the presence of the impurity can lead to two extremes of behavior that have been observed experimentally. These have been called one- and two-mode behavior.[1] A mixed crystal $A_{0.5}B_{0.5}$ that shows one-mode behavior typically has one strong phonon mode in its infrared spectrum occurring at a frequency intermediate to the relevant mode frequencies $\omega_A$ and $\omega_B$ of the pure crystals $A$ and $B$. If $A_yB_{1-y}$ exhibits two-mode behavior, then $A_{0.5}B_{0.5}$ will have two strong modes whose frequencies are close to $\omega_A$ and $\omega_B$. The present study of $KNi_yMg_{1-y}F_3$ examines the infrared modes in a mixed perovskite that has three infrared-active modes at $y=0$ and at $y=1$. For intermediate $y$ two of these show one-mode behavior and one of these shows two-mode behavior. This is the first report of a systematic study of a system that simultaneously exhibits both kinds of behavior.

A simple model that includes effective charges and inter-ion force constants but neglects local-field effects is used to analyze the results. This model leads quite naturally to the behavior observed experimentally with a minimum number of special assumptions.

In Sec. II, the experimental methods and results are described. Section III presents the model of the long-wavelength lattice vibrations in the mixed crystal and the method for calculating the corresponding dielectric function for analysis of the optical properties. In Sec. IV, the model is compared with experiment and a discussion is given of the model parameters and normal modes.

## II. EXPERIMENTAL METHODS AND RESULTS

### A. Sample Preparation

The crystals were grown by a modified Stockbarger method in sealed platinum systems.[4] Single crystals of $KNiF_3$ and $KMgF_3$ were used as starting material. These materials form solid solutions at all concentrations and single crystals $12\times12\times5$ mm were easily obtained.

[1] H. W. Verleur and A. S. Barker, Jr., Phys. Rev. **164**, 1169 (1967).
[2] I. F. Chang and S. S. Mitra, Phys. Rev. **172**, 924 (1968).
[3] In addition to Refs. 1 and 2, review papers on mixed crystals appear in *Proceedings of International Conference on Localized Excitation in Solids*, edited by R. F. Wallis (Plenum Press, Inc., New York, 1968).
[4] H. J. Guggenheim, J. Phys. Chem. **64**, 938 (1960).

### B. Measurements

Room-temperature reflectivity and transmission measurements in the region 280–10 000 $cm^{-1}$ were made, using a double-pass prism spectrometer.[5] For measurements in the region 140–280 $cm^{-1}$ a far-infrared grating spectrometer was used, employing a helium-cooled germanium bolometer as the detector. Reflectivity measurements were made by comparing the reflected signal from a freshly aluminized front-surface mirror with that from the polished surface of the crystal being examined. The mirror and crystal were mounted side by side on a traveling sample holder. Transmission measurements were made using a Dewar with CsBr or polyethylene windows, depending on the wavelength. In this case the crystal was mounted to a copper cold finger by means of conducting silver cement. The entire cold finger was enclosed in a low-temperature heat shield containing ports that allow only the radiation from the spectrometer to enter and leave the experimental sample region. For transmission measurements the amount of radiation passing through the crystal was compared with that passing through a masked-down port of the same dimension. The sample temperature could be held at 300, 80, or 25°K.

Surface preparation of the crystals used for both reflectivity and transmission measurements include lapping on AO 303½ (11 $\mu$ size) and AO 305 (3 $\mu$ size) abrasive with the final polish on 1 $\mu$ diamond compound.

### C. Results and Analysis

In Fig. 1, the reflectivity results are shown for the pure and mixed crystals. Most measurements were carried up to 10 000 $cm^{-1}$; however, no structure was observed above 600 $cm^{-1}$. The limiting value of the reflectivity as it flattens out near 10 000 $cm^{-1}$ was used to calculate the high-frequency dielectric constant $\epsilon_\infty$. Values of $\epsilon_\infty$ are given in each figure. From Fig. 1 we see that there are three fundamental transverse and three fundamental longitudinal lattice modes in the two pure crystals. Additional weak modes are also detected superimposed on the highest-frequency reststrahlen bands. Such weak modes are marked with an asterisk wherever they occur. For the mixed crystals there is an additional transverse and longitudinal mode pair that gives quite pronounced structure to the intermediate reststrahlen band.

The data shown in Fig. 1 have been analyzed by fitting the reflectivity using classical oscillators for the

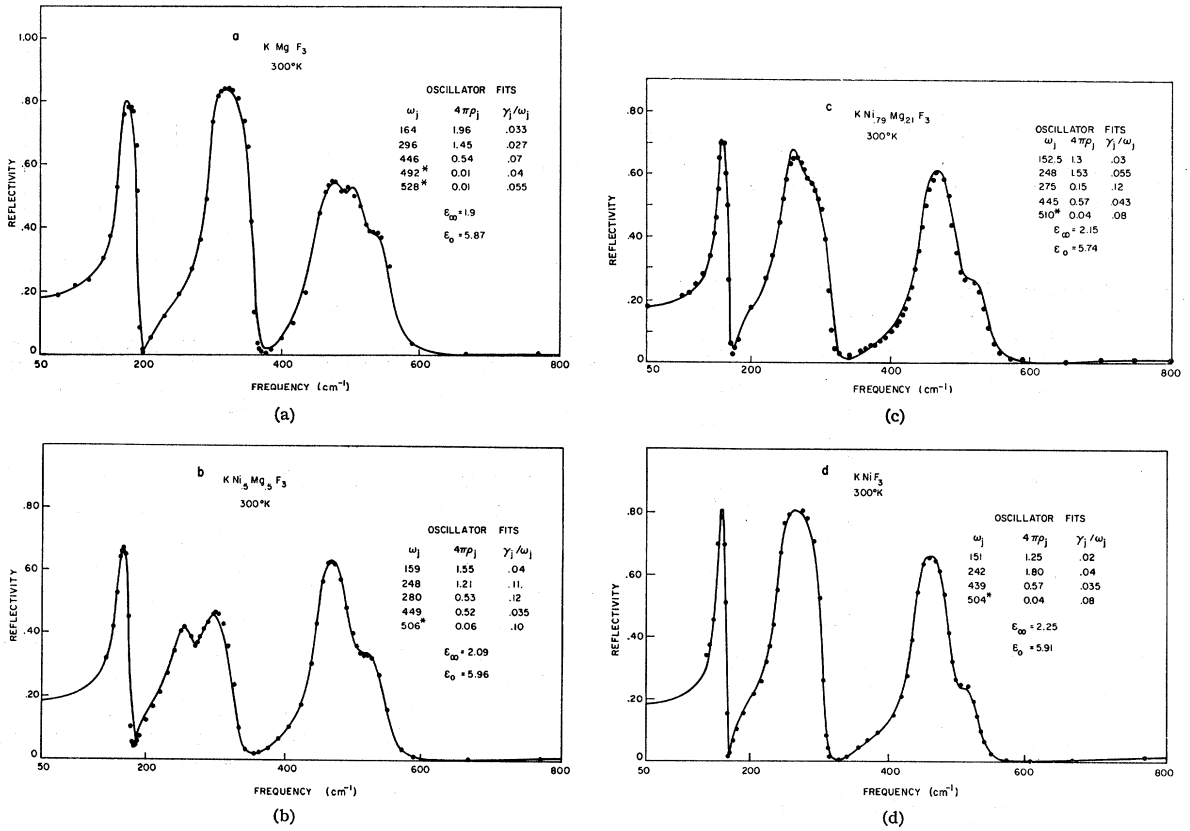


FIG. 1. Reflection spectra of the mixed crystals. The points show the experimental measurements. The solid curves are oscillator fits whose corresponding parameters are given in each figure.

[5] W. G. Spitzer and D. A. Kleinman, Phys. Rev. **121**, 1324 (1961).

optic modes.[5] We assume that the dielectric function $\epsilon(\omega)$ can be represented by

$$\epsilon(\omega)=\epsilon_\infty+\sum_j \frac{4\pi\rho_j\omega_j^2}{\omega_j^2-\omega^2+i\omega\gamma_j}. \quad (1)$$

The reflectivity is calculated from Eq. (1), using trial parameters for $\epsilon_\infty$ and $\omega_j$, $4\pi\rho_j$, and $\gamma_j$. We proceed by adjusting these parameters until a good fit is achieved. This method has been discussed extensively by others.[5] The solid curves in Fig. 1 show the best fits using this method. The corresponding parameters are given in the figures.

In preparation for the discussion of the modes in the mixed crystals, we analyze Eq. (1) for the longitudinal optic (LO) mode frequencies $\omega_l$. It is worth emphasizing that, once we have adopted Eq. (1), we can specify the transverse frequencies and strengths as independent parameters (as listed in Fig. 1) or we can just as easily consider the transverse frequencies and longitudinal frequencies as independent parameters. The longitudinal phonon frequencies occur where $\epsilon=0$.[6] In general, the solutions of $\epsilon=0$ are complex; however, in all cases the imaginary part of the frequency is less than 3% of the real part, allowing us to visualize these modes as lightly damped longitudinal lattice vibrations. In Table I, we list the absolute value of the longitudinal phonon frequencies as well as the $\omega_j$ of Eq. (1). We take $\omega_j$ as the transverse phonon frequencies and, as mentioned above, we can take all the parameters in Table I together with the imaginary parts of the $\omega_l$ (not shown) to specify the optical behavior of the crystals. In the table, we again denote weak modes with an asterisk.

TABLE I. Experimental transverse and longitudinal infrared phonon frequencies at $T=300°K$. An asterisk denotes weak mode forbidden in first order.

| $KMgF_3$ | | $KNi_{0.2}Mg_{0.8}F_3$ | |
|---|---|---|---|
| $\omega_{TO}$ | $\omega_{LO}$ | $\omega_{TO}$ | $\omega_{LO}$ |
| 164 | 192 | 165 | 188 |
| 296 | 360 | 253 | 258 |
| 446 | 490* | 298 | 350 |
| 492* | 522* | 454 | 492*[a] |
| 530* | 550 | 495* | 517*[a] |
| | | 526* | 557[a] |
| $KNi_{0.5}Mg_{0.5}F_3$ | | $KNi_{0.79}Mg_{0.21}F_3$ | |
| 159 | 178 | 152 | 168 |
| 248 | 266 | 248 | 271 |
| 280 | 330 | 275 | 315 |
| 449 | 495* | 445 | 498* |
| 506* | 547 | 510* | 536 |
| $KNiF_3$ | | | |
| 151 | 165 | | |
| 242 | 306 | | |
| 439 | 491* | | |
| 504* | 527 | | |

[a] Data for this crystal were taken from Perry and Young (Ref. 7). They did not analyze for the weak longitudinal components; therefore their data have been reanalyzed to give new values for these modes and the raising of their 547 mode to 557 $cm^{-1}$.

[6] A. S. Barker, Jr., Phys. Rev. **136**, 1290 (1964).

In Figs. 2 and 3, we show the transmission spectra of two thin samples of the mixed crystal for $y$ near zero. The two major dips in transmission correspond to the lowest and the intermediate reststrahlen modes of $KMgF_3$. The presence of Ni causes extra absorption. Oscillator fits were carried out here also. The solid curves in Figs. 2 and 3 show these fits. Equation (1) is used to describe the dielectric function of the sample, and standard film transmission formulas are used. One additional weak mode is used in Eq. (1) to describe mixed-crystal modes due to Ni. The oscillator parameters are given in Table II. Note that the best-fit parameters to the main modes differ somewhat from those given in Fig. 1 for pure $KMgF_3$. Real differences can be expected for the cooled runs, since damping tends to decrease, and restoring forces to increase, on cooling.

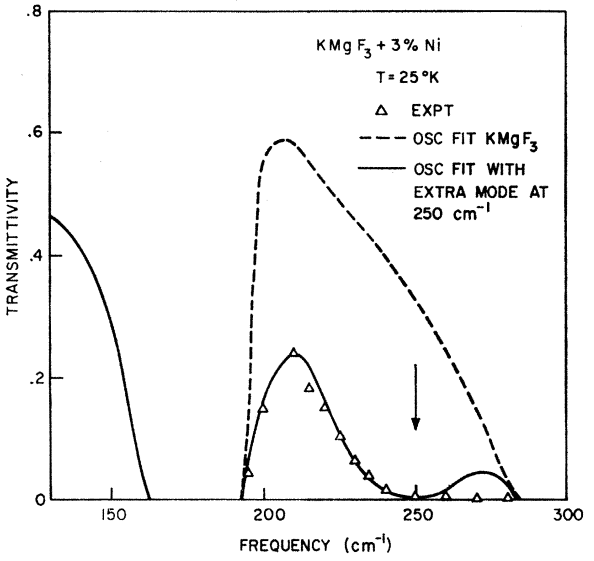


FIG. 2. Transmission spectrum $KMgF_3$ with 3% of Mg replaced with Ni. Sample thickness is 0.13 mm. The solid curve corresponds to an oscillator fit that includes an extra mode for the vibrations caused by the presence of Ni.

Such differences are seen in Table II. In addition, even at room temperature there are differences between the mode parameters determined by transmission and by reflection experiments. The differences noted in this study are typical of this kind of discrepancy for infrared-active phonons. They occur because Eq. (1) for $\epsilon(\omega)$ is not a perfect description of the optical properties. Transmission measurements for thickness $\sim$0.1 mm are more sensitive to the form of $\epsilon$ several linewidths away from $\omega_j$, while reflection experiments are sensitive to the shape of $\epsilon$ very near $\omega_j$. While the discrepancy is barely larger than the intrinsic uncertainties in measuring the mode parameters, in this study we use wherever possible the reflectivity analysis of mode parameters for consistency.

In general, throughout the concentration range the

presence of Ni in KMgF causes one extra mode that can be seen in reflection for $y>0.20$ and in transmission for $y<0.05$. For $y=0.79$ the extra (fourth) mode is difficult to detect. Figure 4 shows a Kramers-Kronig analysis of the reflectivity for $y=0.79$ and 1.0. The mode for pure nickel ($y=1.0$) is shifted in Fig. 4 to be on top of the mixed-crystal mode. The presence of Mg causes the raised shoulder (dashed curve) 30 $cm^{-1}$ above the main mixed-crystal mode. Rather than trying to resolve the Kramers-Kronig value of $\epsilon''$ into two modes, we fitted the reflectivity (Fig. 1) with an additional mode about 30 $cm^{-1}$ above the main mode. This weak mode is shown as an insert in Fig. 4 for comparison with the over-all combined-mode shape.

The appearance of an extra mode in the mixed crystals has also been noted by Perry and Young[7] for

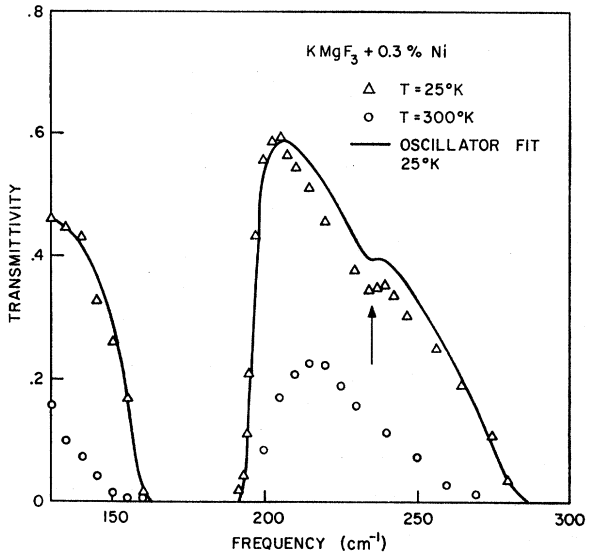


FIG. 3. Transmission spectrum of $KMgF_3$ with 0.3% of Mg replaced with Ni. Sample thickness is 0.13 mm. The solid curve is an oscillator fit that contains a weak mode (Table II) to reproduce the dip near 230 $cm^{-1}$.

two of the compositions studied by the present authors. Data from their sample with $y=0.2$ will be included in our analysis to give uniform coverage of the concentration range $y=0$–1.0.

## III. LATTICE-VIBRATION MODEL

### A. Description of Model and Evaluation for Pure Crystals

A pure perovskite crystal has five ions in the primitive unit cell. The point group is $O_h$. A consideration of the group characters for ion motion along a principal axis shows that for long-wavelength vibrations there are four $T_{1u}$ ($\Gamma_{15}$)-type and one $T_{2u}$ ($\Gamma_{25}$)-type modes. The ion displacements for the $T_{2u}$ mode and for one of

[7] C. H. Perry and E. F. Young, J. Appl. Phys. 38, 4616 (1967).

TABLE II. Oscillator parameters used to fit transmission measurements at low nickel concentrations.

| $T=300°K$ | | | $T=25°K$ | | |
|---|---|---|---|---|---|
| $\omega_j$ | $4\pi\rho_j$ | $\gamma_j$ | $\omega_j$ | $4\pi\rho_j$ | $\gamma_j$ |
| | | $KMgF_3$:Ni ($y=0.003$) | | | |
| 161 | 1.8 | 0.02 | 166 | 1.8 | 0.0025 |
| 300 | 1.45 | 0.017 | 300 | 1.45 | 0.005 |
| Weak mode too broad to be determined | | | 235 | 0.001 | 0.06 |
| | | $KMgF_3$:Ni ($y=0.03$) | | | |
| 161 | 1.8 | 0.02 | 166 | 1.9 | 0.003 |
| 300 | 1.45 | 0.017 | 300 | 1.45 | 0.005 |
| Weak mode too broad to be determined | | | 250±12 | 0.08 | 0.12 |

the $T_{1u}$ modes (the acoustic mode) are easily written. The displacements for the remaining three infrared-active $T_{1u}$ modes cannot be determined by group theory, i.e., they are model-dependent. Several possible mode-displacement vectors are given below.

The occurrence of five ions in the perovskite unit cell allows the introduction of many more force, charge, and polarizability parameters than are needed in a model of an NaCl-type crystal. For these latter diatomic crystals quite satisfactory shell models can be constructed that reproduce the sound-wave velocities and

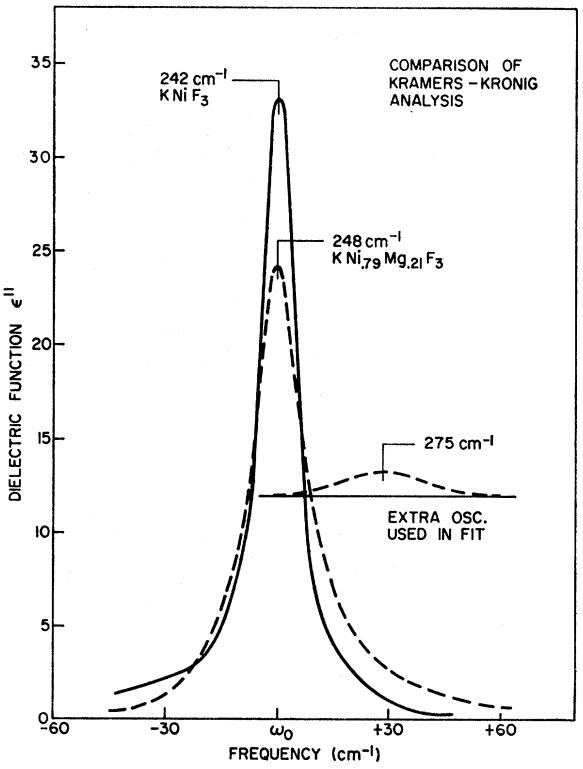


FIG. 4. Comparison of Kramers-Kronig analysis of pure $KNiF_3$ with $KNi_{0.79}Mg_{0.21}F_3$. The mixed crystal shows a broad region of extra absorption 30 $cm^{-1}$ above the main mode. The dashed curve labeled Extra Osc. shows the fitted form of this extra absorption from the fit of Fig. 1(c).

the first-order infrared and neutron-phonon spectra.[8] Cowley has fitted several shell models to the perovskite $SrTiO_3$.[9] Contrary to the satisfactory state of affairs in the NaCl-type crystals, he has found that several different models work fairly well, but no one model fits all the experimental results ideally. Joseph and Silverman have also fitted certain $SrTiO_3$ phonon data using a very simple model.[10] They also found that more than one model (i.e., more than one set of force constants) would fit the observed frequencies. We have followed their approach, using a rigid-ion model with three force constants, but have included charge effects to evaluate the mode strengths (or, equivalently, the LO mode frequencies) as well as the transverse optic (TO) mode frequencies. We also obtain several solutions; however, the ion charges are quite unreasonable for some of the models, which allows a choice to be made of the most realistic model. Axe has recently described such reasonable models for several perovskites and we make comparisons with his work where appropriate.[11]

Figure 5 shows a unit cell of $KNi_yMg_{1-y}F_3$. The framework of K and F ions remains translationally invariant through the crystal except for small distortions due to the slightly different ionic radii of Ni and Mg. At the center of each cell either an Ni or Mg ion may occur. We number the ions as shown in Fig. 5 and introduce three independent force constants. For long-wavelength vibrations seven independent ion coupling constants can be defined.[10] The problem is overspecified, of course, since there are only four optical-mode frequencies. For long wavelengths the force constants are best viewed as sublattice coupling constants. Of the seven independent constants, it can be easily seen that only four are associated with nearest-neighbor bonds. Of these four, two are bond-bending–type force constants and are expected to be somewhat weaker than the other two bond-stretching force constants. For simplicity, we set one of the nearest-neighbor bond-bending force constants equal to zero and all second- and higher-neighbor force constants equal to zero to retain a three-parameter problem.[10] For pure $KNiF_3$ the force constants are $k_{12}$, $k_{25}$, and $k_{45}$, where the subscripts indicate the ions being linked. The corresponding constants for pure $KMgF_3$ are $k_{12}$, $k_{26}$, and $k_{46}$. For a mixed crystal both types of bond will occur. For example, an F ion might be linked to an Mg on one side ($k_{26}$) and to an Ni ion ($k_{25}$) on the other side. In addition to these force constants, we can include a third-neighbor force constant or bond $k_{56}$ linking Ni and Mg ions when they occupy adjacent cells in a mixed crystal. There are four other force constants equivalent by symmetry to those above, such as $k_{13}=k_{12}$, $k_{35}=k_{25}$, etc.

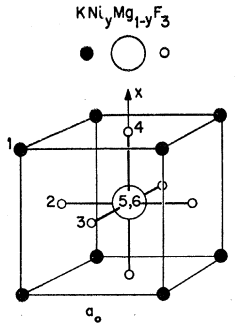


FIG. 5. Unit cell of $KNi_yMg_{1-y}F_3$. The central ion is Ni (or Mg) with probability $y$ (or $1-y$).

For the vibration direction shown in Fig. 5, F ion 4 is not equivalent to F ions 2 and 3. We thus assign ion charges $Z_i$, $i=1$–5, with $z_2=z_3\neq z_4$ and $\sum_i z_i=0$. We consider in detail the derivation of only one equation of motion. The methods used have been described previously.[1] When ion 5 is displaced along $x$ (Fig. 5), it experiences restoring forces from its bonds with ions 2, 3, 4, and 6. The equation of motion is

$$m_5\ddot{x}_5=-(x_5-x_2)k_{25}-(x_5-x_3)k_{25}-(x_5-x_4)k_{45}-(1-y)(x_5-x_6)k_{56}+z_5E, \quad (2)$$

where $y$ is the Ni concentration and $E$ is the electric field. The first three terms on the right side of Eq. (2) come from ions that always surround an Ni ion. We assume a random distribution of Mg ions; thus the fourth term gives a probability-weighted force due to the presence of Mg at the sites adjacent to an Ni ion. We take $E$ to be the macroscopic electric field, i.e., we assume that local-field effects can be included in the force and charge parameters. Equation (2) is multiplied through by $y$ (and the equation for $x_6$ by $1-y$) to give the following matrix equation for the long-wavelength lattice-vibration problem:

$$\mathbf{m}\ddot{\mathbf{x}}=\mathbf{k}\mathbf{x}+\mathbf{z}E, \quad (3)$$

where $\mathbf{m}$ is the diagonal mass matrix

$$\mathbf{m}=\begin{bmatrix} m_1 & & & & & \\ & m_2 & & & 0 & \\ & & m_3 & & & \\ & & & m_4 & & \\ & & 0 & & ym_5 & \\ & & & & & (1-y)m_6 \end{bmatrix} \quad (4)$$

and $\mathbf{x}$ and $\mathbf{z}$ are the displacement and charge vectors

$$\mathbf{x}=\begin{bmatrix} x_1 \\ x_2 \\ x_3 \\ x_4 \\ x_5 \\ x_6 \end{bmatrix}, \quad \mathbf{z}=\begin{bmatrix} z_1 \\ z_2 \\ z_3 \\ z_4 \\ (y)z_5 \\ (1-y)z_6 \end{bmatrix}. \quad (5)$$

[8] A. D. B. Woods, B. N. Brockhouse, R. A. Cowley, and W. Cochran, Phys. Rev. **131**, 1025 (1963).
[9] R. A. Cowley, Phys. Rev. **134**, A981 (1964).
[10] R. I. Joseph and B. D. Silverman, J. Phys. Chem. Solids **24**, 1349 (1963).
[11] J. D. Axe, Phys. Rev. **157**, 429 (1967).

The dynamical matrix is

$$\mathbf{k}=\begin{bmatrix} -(2k_{12}) & k_{12} & k_{12} & 0 & 0 & 0 \\ & -[yk_{25}+(1-y)k_{26}] & 0 & 0 & yk_{25} & (1-y)k_{26} \\ & & -[yk_{25}+(1-y)k_{26}] & 0 & yk_{25} & (1-y)k_{26} \\ & & & -[yk_{45}+(1-y)k_{46}] & yk_{45} & (1-y)k_{46} \\ & & & & -y[2k_{25}+k_{45}+(1-y)k_{56}] & y(1-y)k_{56} \\ k_{ij}=k_{ji} & & & & & -(1-y)(2k_{26}+k_{46}+yk_{56}) \end{bmatrix}. \quad (6)$$

To discuss mode strength, we need the polarization equation

$$P=(1/v)[z_1x_1+z_2x_2+z_3x_3+z_4x_4+yz_5x_5 +(1-y)z_yx_6]+[(\epsilon_\infty-1)/4\pi]E, \quad (7)$$

where $e$ and $v$ are the electron charge and unit-cell volume. We have again used the random-probability coefficients for ions 5 and 6 in the obvious way. $\epsilon_\infty-1$ describes the frequency-independent part of the polarization due to higher-frequency electronic effects.

Equation (7) may be solved to give the polarization in terms of the driving electric field that we take to have the form $Ee^{i\omega t}$. The dielectric function may be evaluated from the definition

$$\epsilon=1+4\pi P/E. \quad (8)$$

The simple harmonic theory outlined above gives a dielectric function $\epsilon(\omega)$ with modes or resonances of simple classical oscillator form [Eq. (1)]. For each mode we now introduce an *ad hoc* damping coefficient $\gamma_j$ to obtain Eq. (1) used earlier to fit the experimental data. To reiterate: For a given set of force constants and charges, and a particular concentration $y$, Eqs. (3)–(8) may be solved to yield the $\omega_j$ and $4\pi\rho_j$, i.e., the mode frequencies and strengths. It may be shown fairly readily that the six equations of motion give one zero-frequency (acoustic) mode and one infrared-inactive ($T_{2u}$ type with $4\pi\rho_j=0$) optic mode. The remaining four modes are infrared-active. Equation (1) for $\epsilon(\omega)$ containing $\omega_j$ and $4\pi\rho_j$, $j=1$–4, may then be compared with experiment. Our actual fitting procedure will be discussed below. Table III gives the best-fit model parameters at $y=0$ and 1, i.e., for the pure fluoride crystals.

Before proceeding to the mixed-crystal lattice vibrations, we should note several features of the solutions at $y=0$ and 1 that are given in Table III. Joseph and Silverman have given a description of the inversion of the dynamical matrix to obtain the force constants from the experimental frequencies. Since we have a sixth-order secular equation for the three infrared modes, we can obtain as many as six sets of real force constants, i.e., as many as six different models. At $y=0$ ($KMgF_3$), we find two models, i.e., two sets of force constants that give the observed infrared transverse frequencies. For $KNiF_3$ there are four models. $KMgF_3$ model 1 was eliminated because, when combined with any of the four $KNiF_3$ models to predict mixed-crystal behavior, frequencies tried to cross as $y$ was varied, contrary to experiment. This model also had quite unreasonable effective charges. The four $KNiF_3$ models were studied in the mixed crystal and only two give reasonable

TABLE III. Model parameters and mode frequencies, strengths, and displacements for the pure crystals.

$KMgF_3$ (model 1)

| Forces ($10^5$ dyn/cm) | | | $k_{12}=0.670$ | | $k_{26}=0.632$ | $k_{46}=0.327$ | |
|---|---|---|---|---|---|---|---|
| Charges ($\|e\|$) | | | $z_1$ | $z_2$ | $z_3$ | $z_4$ | $z_6$ |
| | | | +0.009 | −0.38 | −0.38 | −1.64 | +2.391 |
| Formal valence ($\|e\|$) | | | +1.0 | −1.0 | −1.0 | −1.0 | +2.0 |
| Frequency ($cm^{-1}$) | Strength | Type | K | $F_2$ | $F_3$ | $F_4$ | Mg |
| $\omega_1=0$ | 0 | Acoustic | 0.070 | 0.070 | 0.070 | 0.070 | 0.070 |
| $\omega_2=164$ | 1.96 | IR | −0.054 | −0.029 | −0.029 | 0.154 | 0.012 |
| $\omega_3=296$ | 1.28 | IR | 0.078 | −0.040 | −0.040 | 0.051 | −0.102 |
| $\omega_4=340$ | 0 | Inactive | 0.000 | 0.125 | −0.125 | 0.000 | 0.000 |
| $\omega_5=446$ | 0.67 | IR | 0.038 | −0.091 | −0.091 | −0.016 | 0.095 |

$KNiF_3$ (model B)

| Forces | | | $k_{12}=0.601$ | | $k_{25}=0.947$ | $k_{45}=0.242$ | |
|---|---|---|---|---|---|---|---|
| Charges | | | $z_1$ | $z_2$ | $z_3$ | $z_4$ | $z_5$ |
| | | | −0.49 | −0.77 | −0.77 | −1.16 | 3.19 |
| Frequency ($cm^{-1}$) | Strength | Type | K | $F_2$ | $F_3$ | $F_4$ | Ni |
| $\omega_1=0$ | 0 | Acoustic | 0.062 | 0.062 | 0.062 | 0.062 | 0.062 |
| $\omega_2=149$ | 1.24 | IR | −0.044 | −0.025 | −0.025 | 0.161 | 0.006 |
| $\omega_3=240$ | 1.79 | IR | −0.089 | 0.010 | 0.010 | −0.039 | 0.066 |
| $\omega_4=371$ | 0 | Inactive | 0.000 | −0.125 | 0.125 | 0.000 | 0.000 |
| $\omega_5=439$ | 0.56 | IR | 0.039 | −0.106 | −0.106 | −0.006 | 0.044 |

results. Of these two, one proved much better (model B) than the other in fitting the experimental data, and it is described in detail.

Most models gave a lowest-frequency optic-mode vibrational pattern somewhat like the K-versus-$MgF_3$ (or K-versus-$NiF_3$) type suggested by Last[12] and by Perry *et al.*[13]; however, it was not exactly of this type, nor should we expect it to be this simple. Axe has given a discussion of the form of the displacement pattern that can be expected in oxide and fluoride perovskites.[11] From Table III we note also that the vibrational pattern for any particular infrared mode is different in the two pure crystals for the models presented. We expect, therefore, that simple virtual-ion models[1] cannot be applied individually to each mode to predict its concentration dependence in the mixed crystal.

For the pure crystals shown in Table III, and for the mixed crystals (see below), we always obtain a $T_{2u}$ inactive mode ($\omega_4$ for the two models shown) at a certain frequency, depending on the three force constants. Since the $T_{2u}$ mode is orthogonal to all the other modes, at any time we can introduce an additional constant $k_{23}$ (bond bending) that will affect the $T_{2u}$ mode but leave all other frequencies unchanged. Since such forces may be significant in the crystal, high confidence cannot be attached to the frequency predicted for this mode in the present model. If data on this mode became available, we could always fit it with one additional parameter without changing the infrared modes.

Finally, we should comment on the effective charges for the pure crystals. In Table III, we show these charges and the usual valence charge associated with the ions. Axe, in his treatment of several perovskites, fixes the ratio $z_5/z_1$ (or $z_6/z_1$ for $KMgF_3$) at 2.0, which is the ratio of the formal valence charges.[11] With our model we allow all the charges to vary, with the one restriction that $\sum z_j=0$. We use a least-squares-fitting procedure that is simple, since our model with no local fields has phonon frequencies independent of the charges. We thus vary $z_j$ to fit the three mode strengths. The charges were similar to those of Axe; however, for six of the eight models $z_5/z_1$ was much greater than 2. Cowley's models for $SrTiO_3$ have $z_5/z_1$ ranging from 1.5 to 6.[9] For the models chosen here $z_1$ was quite small and actually changed sign and became negative in $KNiF_3$. We do not think that a negative effective charge for the potassium ion necessarily invalidates the model, but it may be the result of our somewhat restrictive procedure of describing the dynamics with a few effective parameters. We note that fairly reasonable mode strengths can be obtained with the potassium charge fixed at a positive value; however, for a best fit to the data we allow it to be negative in model B. The average discrepancy of the mode strengths from experiment was $\langle 4\pi\rho(\text{model})-4\pi\rho(\text{expt})\rangle_{\text{av}}\leq 0.2$. The final charges and the mode strengths that they produce are listed in Table III.

### B. Model for Mixed Crystals

For mixed crystals we must evaluate Eq. (3) for intermediate values of the concentration $y$. We note immediately one inconsistency in the force matrix (6). We must insert a value for the potassium-fluorine force constant $k_{12}$. Table III shows that this force has a different value in the two pure crystals. We expect this behavior in general. There is no reason that forces should remain the same while foreign atoms are added to the system. When 100% Ni replaces Mg in $KMgF_3$, it stretches the lattice parameter from 4.00 to 4.01 Å. We note that $k_{12}$ drops about 10% (Table III), which is a change in the direction that we would expect.

Without adding new parameters to the problem, it is reasonable to take a concentration-dependent force constant[14]

$$k_{12}=yk_{12}(KNiF_3)+(1-y)k_{12}(KMgF_3)$$
$$=y(0.601\times 10^5)+(1-y)(0.67\times 10^5). \quad (9)$$

Similarly, the polarization equation requires charges for each of the ions. We use the above assumption for the potassium and fluorine ion charges:

$$z_j=yz_j(KNiF_3)+(1-y)z_j(KMgF_3), \quad j=1, 4. \quad (10)$$

So far we have used only constants available from the pure-crystal data and some reasonable assumptions involving the interpolation of forces and charges between the pure-crystal values. A model based on these parameters alone has been evaluated. It gives a good fit at $y=0$ and 1 but a rather poor fit at $y=0.5$. The reason is fairly obvious. We have not considered modification of the fluorine-magnesium forces as nickel is added. We cannot interpolate, since this force is absent in pure $KNiF_3$. One way of viewing this problem is to ask whether we know what forces control the vibration of an isolated Ni ion in $KMgF_3$. The mass-defect model often used to predict local modes would say that the Ni force is the same as the Mg forces that existed before the Mg was replaced. This model works poorly here and for most cases that have been investigated.[15] We must actually deal with force and mass changes when Ni is added to $KMgF_3$ (or Mg is added to $KNiF_3$).

We therefore must include additional parameters.

---

[12] J. T. Last, Phys. Rev. **105**, 1740 (1957).

[13] C. H. Perry, B. N. Khanna, and G. Rupprecht, Phys. Rev. **135**, A408 (1964).

[14] Y. S. Chen, W. Shockley, and G. L. Pearson, Phys. Rev. **151**, 648 (1966). These authors used concentration-dependent forces for $GaAs_yP_{1-y}$. They note the relation to Grüneisen's law and make an estimate of the expected bond changes from thermodynamic data.

[15] A. J. Sievers, in *Proceedings of International Conference on Localized Excitation in Solids*, edited by R. F. Wallis (Plenum Press, Inc., New York, 1968).

We write

$$k_{25}=[1+(1-y)\lambda]k_{25}(KNiF_3),$$
$$k_{45}=[1+(1-y)\lambda]k_{45}(KNiF_3),$$
$$k_{26}=(1+y\delta)k_{26}(KMgF_3),$$
$$k_{46}=(1+y\delta)k_{46}(KMgF_3), \quad (11)$$

i.e., introduce two parameters $\lambda$ and $\delta$ that give the fractional change in bond strength as impurity ions are added. Chen *et al.* have used the same approach in mixed GaAs-GaP.[14] Since the addition of Ni stretches the lattice, we expect $\lambda$ to be positive and $\delta$ to be negative. This is found to be the case and both $\lambda$ and $\delta$ have a magnitude of about 0.2. $\lambda$ and $\delta$ may both be evaluated from the $y=0.5$ experimental data; thus we are not over parametrized, since we have data for four remaining concentrations to compare with the model.

In Fig. 6, we show the experimental results and model calculations for all concentrations. Rather than showing the transverse-mode frequencies and strengths, we plot the transverse- and longitudinal-mode frequencies. The points show the transverse and longitudinal modes found experimentally. The weak forbidden modes near 500 $cm^{-1}$ are not included. The curves show the modes predicted by model B1 which has the parameters given in Table III plus the constants $\lambda=0.17$, $\delta=-0.26$, and $k_{56}=-0.15\times10^5$ dyn/cm. The most obvious discrepancy between the model and experiment appears for the highest-frequency LO mode. This arises for two reasons not related to the basic dynamics. First, all crystals show weak forbidden modes near 500 $cm^{-1}$ that push the highest longitudinal mode up by 15–20 $cm^{-1}$. We could add such modes to the model, improving the agreement for all concentrations except $y=0.0$ and 0.03. Here the model is known to give too high an LO mode frequency. This occurs simply because the mode strength $4\pi\rho(\omega_5)$ is too large ($4\pi\rho=0.67$ for the charges used). The actual mode strength measured experimentally is 0.54 for $KMgF_3$ [Fig. 1(a)]. Thus our fit to the charges that was arbitrarily halted when a precision of 0.2 was obtained left the strength of mode $\omega_5$ about as large as a composite mode that includes the main mode and the two forbidden modes in $KMgF_3$. The general fit is quite good, considering the few parameters used to predict the eight modes at all concentrations.

In a situation like this, where there are four transverse modes at intermediate concentrations but only three for each pure crystal, one transverse-longitudinal pair must become degenerate at $y=0$ and another (possibly different pair) at $y=1.0$. We can view this as a cancelling of a pole and a zero in the dielectric function, reducing the Lyddane-Sachs-Teller relation[6] from four mode pairs to three mode pairs. For $y\rightarrow1$ in

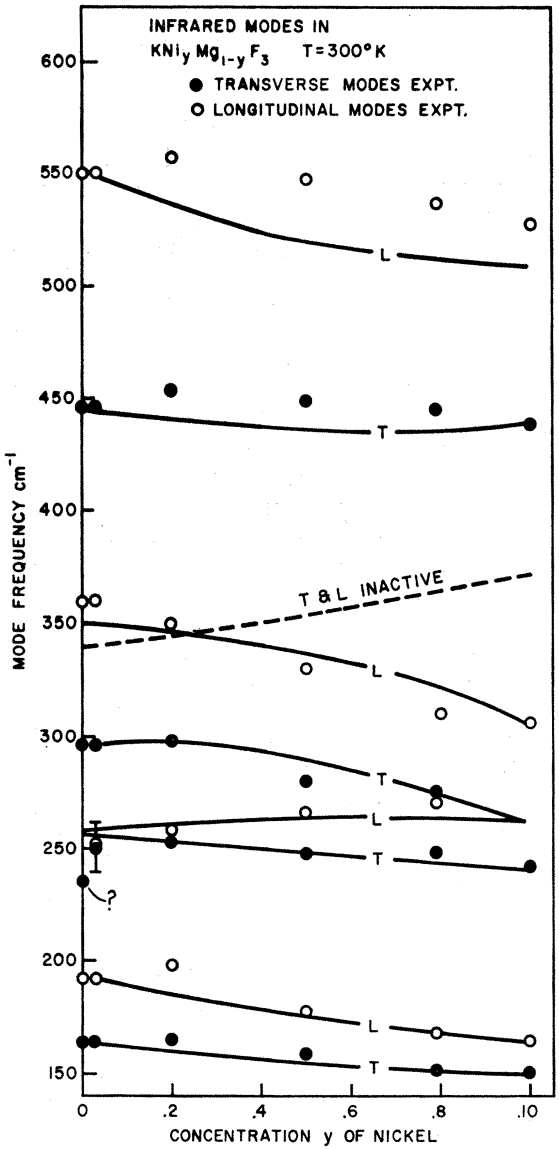


FIG. 6. Mode frequencies for model B-1. The four transverse and four longitudinal infrared vibration modes are shown as solid curves and the inactive mode as a dashed curve. The points give the experimental results for the infrared modes. The closely spaced transverse-longitudinal mode pair labeled ? may not be fundamental vibrations (see text).

$KNi_y$-$Mg_{1-y}F_3$ we find[16]

$$\lim_{y\rightarrow1}\frac{\epsilon_0}{\epsilon_\infty}=\lim_{y\rightarrow1}\frac{\omega_{l1}^2}{\omega_{t1}^2}\frac{\omega_{l2}^2}{\omega_{t2}^2}\frac{\omega_{l3}^2}{\omega_{t3}^2}\frac{\omega_{l4}^2}{\omega_{t4}^2}=\frac{\omega_{l1}^2}{\omega_{t1}^2}\frac{\omega_{l3}^2}{\omega_{t2}^2}\frac{\omega_{l4}^2}{\omega_{t4}^2}. \quad (12)$$

This behavior is completely equivalent to mode $\omega_{t2}$ having its strength shrink to zero at this limiting concentration. Such a weak mode at low concentrations is equivalent to a local or resonant impurity mode de-

[16] For simplicity, we set all damping constants equal to zero. A slightly modified form of Eq. (12) must be used for finite damping.

pending on the density of phonon states at its frequency. For the present mixed system, the impurity mode near $y=1$ lies at 263 $cm^{-1}$, right under the reststrahlen band (opaque region) of $KNiF_3$. This mode could not therefore be studied for low Mg concentrations. Near $y=0$, the impurity mode near 258 $cm^{-1}$ lies in a fairly transparent region between two reststrahlen bands of $KMgF_3$. This mode was studied at two low concentrations in transmission and fitted with the mode parameters in Table II. At $y=0.03$ the modes are close to those predicted by the model but appear very broad. At $y=0.003$ a weak mode was found about 20 $cm^{-1}$ lower than the frequency predicted by the model. Since we expect no strong concentration dependence between $y=0.003$ and 0.03, this result may indicate that the mode seen is not the impurity mode but a second-order (combination) mode of the host. The very weak mode predicted by the model at $y=0.003$ would be very hard to detect if it was broadened as much as the $y=0.03$ impurity mode that *was* observed unambiguously.

In addition to the infrared-active modes, we plot in Fig. 6 the frequency of the triply degenerate inactive optic mode. As explained earlier, the frequency of this mode may be inaccurate, since it results from force constants that were adjusted to fit all modes but this one. No data (such as neutron spectra) are available yet on the inactive modes.

Table IV shows the ion-displacement patterns for the mixed-crystal infrared modes for several concentrations. The inactive mode has the same displacements at all concentrations as given in Table III for the pure crystals, and is not included. For $y=0.001$ we find that three of the mode patterns are very close to those of pure $KMgF_3$ (Table III), except that there is an Ni ion present in every thousandth cell that is moving also. The impurity mode ($\omega_2=258$ $cm^{-1}$) has the Ni ion moving with very large amplitude relative to its neighbors. By the time we reach $y=0.50$ there is no distinct impurity mode, though there is definitely more motion of the heavy Ni ion in the lower (247-$cm^{-1}$) peak and more motion of Mg in the higher (289-$cm^{-1}$) peak of the central split reststrahlen band.

TABLE IV. Eigenfrequencies and eigenvectors for the transverse infrared modes in mixed $KNi_yMg_{1-y}F_3$ model B1.

| Ions | | K | F | F | Ni | Mg |
|---|---|---|---|---|---|---|
| Displacements | | $X_1$ | $X_2=X_3$ | $X_4$ | $X_5$ | $X_6$ |
| Frequency ($cm^{-1}$) | Strength | | | $y=0.001$ | | |
| 164 | 1.97 | −0.054 | −0.029 | 0.154 | −0.014 | 0.011 |
| 258 | 0.003 | −0.004 | 0.001 | −0.002 | 3.192 | −0.0004 |
| 296 | 1.28 | −0.077 | 0.040 | −0.051 | −0.077 | 0.102 |
| 446 | 0.67 | −0.038 | 0.091 | 0.016 | −0.47 | −0.095 |
| | | | | $y=0.03$ | | |
| 163 | 1.94 | −0.053 | −0.029 | 0.154 | −0.014 | 0.012 |
| 257 | 0.075 | −0.023 | 0.003 | −0.010 | 0.572 | −0.003 |
| 296 | 1.23 | −0.075 | 0.039 | −0.050 | −0.073 | 0.106 |
| 445 | 0.67 | −0.038 | 0.092 | 0.016 | −0.048 | −0.095 |
| | | | | $y=0.20$ | | |
| 160 | 1.8 | −0.051 | −0.028 | 0.155 | −0.013 | 0.014 |
| 253 | 0.41 | −0.052 | 0.007 | −0.022 | 0.202 | −0.009 |
| 296 | 1.00 | −0.060 | 0.033 | −0.044 | −0.054 | 0.133 |
| 440 | 0.63 | −0.040 | 0.095 | 0.014 | −0.049 | −0.091 |
| | | | | $y=0.50$ | | |
| 155 | 1.56 | −0.048 | −0.027 | 0.158 | −0.010 | 0.019 |
| 247 | 0.86 | −0.072 | 0.008 | −0.029 | 0.112 | −0.020 |
| 289 | 0.75 | −0.042 | 0.022 | −0.037 | −0.029 | 0.195 |
| 435 | 0.57 | −0.041 | 0.101 | 0.010 | −0.049 | −0.079 |

## IV. DISCUSSION

Before discussing the mixed-crystal model developed above, it is worth presenting some essentially different approaches to mixed-crystal vibrations. We first note that the long-wavelength vibrations may be discussed macroscopically.[17] An almost trivial model is to suppose that the mixed crystal is badly segregated, so that, even when $y=0.5$, some regions vibrate like pure $KMgF_3$ and some like pure $KNiF_3$. If these regions are large compared with the wavelength of light, we merely average the reflectivity $R$:

$$R(y)=yR(KNiF_3)+(1-y)R(KMgF_3). \quad (13)$$

Such a crystal is rather uninteresting and hardly deserves the name "mixed crystal." This type of crystal would show x-ray lines characteristic of both parent crystals. The present crystal system showed no such x-ray behavior. Note that one characteristic of this average-reflectivity model is that many reflectivity dips should appear, since even with averaging it is hard to eliminate the very sharp dips near the LO modes. No such dips appear in the present system, except that on the top of the center reststrahlen band. It has the wrong frequency, however, to be caused by either of the pure crystals using Eq. (13). A slightly more subtle model that could result from a mixed crystal occurs when there are segregated regions whose dimension is much smaller than a wavelength of the infrared radiation used to detect lattice vibrations. Now the infrared electric field induces currents that flow through several different regions whose responses must be added in a special way. Suppose that both pure materials $A$ and $B$ have the same high-frequency dielectric constant $\epsilon_\infty$ but different phonon parts: $\epsilon_A$ for the $y=1$ pure crystal and $\epsilon_B$ for the $y=0$ pure crystal. In adding small regions of crystal $A$, the topology of the situation matters considerably, since small threadlike regions of material $A$ right through material $B$ can "short out" $\epsilon_B$ behavior at a resonance of $\epsilon_A$. Assuming small islands of material $A$ in material $B$, a simple calculation gives

$$\epsilon(y)=(1-y^{2/3})\epsilon_B + y^{2/3}\epsilon_A\epsilon_B/[(1-y^{1/3})\epsilon_B+y^{1/3}\epsilon_A]+\epsilon_\infty. \quad (14)$$

Remembering that $y$ gives essentially the volume of impurity type $A$, then $y^{2/3}$ represents the impurity "area" and $y^{1/3}$ its "length." The first term comes from

[17] M. Born and K. Huang, *Dynamical Theory of Crystal Lattices* (Oxford University Press, London, 1954).

the host material directly, while the second term comes from a parallel region of materials $A$ and $B$ in series. Equation (14) has resonances where $\epsilon_B$ has poles and where the weighted sum of $\epsilon_A$ and $\epsilon_B$ has zeros. While Eq. (14) is somewhat suspect because its derivation depends on the shape of the regions of the low-concentration constituent, we find that an evaluation at $y=0.5$ for regions of $KMgF_3$ and $KNiF_3$ near 300 $cm^{-1}$ gives *three* strong modes rather than the two actually observed. Again we might expect x rays to show lines characteristic of both materials. This model is therefore also inapplicable to the present mixed crystals.

A third model that explains the gross features of some mixed crystals of the one-mode type is the virtual- or mean-ion model.[1,18] For the infrared reflectivity we take the dielectric function as given by Eq. (1) but substitute average values for each resonance parameter:

$$\epsilon\sim\langle 4\pi\rho_j\rangle/(\langle\omega_j^2\rangle-\omega^2+i\omega\langle\gamma_j\rangle)\,, \qquad (15)$$

where the brackets denote concentration averaging. For the lowest-frequency mode in the $KNi_yMg_{1-y}F_3$ system we would take

$$\langle\omega_1^2\rangle=y(151)^2+(1-y)(164)^2\,,$$

using frequency units of $cm^{-1}$. Similar averages are formed for $4\pi\rho_1$ and $\gamma_1$. This model gives quite good agreement with experiment for the lowest- and highest-frequency optic modes. Fits to other crystals using this model have been discussed previously.[1] This virtual-ion model fails for the central modes in $KNi_yMg_{1-y}F_3$, however, giving one reststrahlen band instead of two. We note also that even for the lowest and highest modes that experimentally have concentration dependences that are "virtual-ion-like," our model (Table IV) shows that the Mg and Ni ions do not necessarily move together as implied by a microscopic virtual-ion model. Our own view is that virtual-ion models artificially suppress degrees of freedom that are present in a mixed crystal. The models may correctly predict the strongest features in first-order infrared or neutron spectra for some crystals but cannot give weaker modes or fine structure and should be regarded with reservation until all possible lattice-vibration data have been measured.

We now consider microscopic models of the long-wavelength lattice vibrations in mixed crystals. Some calculations have been carried out for linear chains of mixed diatomic crystals by Dean.[19] He considers typically a chain of 30 000 ions, and thus has 30 000 degrees of freedom and must diagonalize rather large matrices. Among the many modes for such a chain are some that can be recognized to have long-wavelength displacement patterns and large dipole strength. We have studied much shorter chains (20 ions) in some detail and find the same result. There are modes with large dipole strength that have similar ions moving in unison. This observation is the basis of the model presented here for $KNiF_3$-$KMgF_3$ and used earlier for GaAs-GaP, $BaF_2$-$SrF_2$,[1] and other mixed crystals.[3] For pure $KNiF_3$ we obviously need five coordinates for long-wavelength vibrations. When some Mg is added, it requires an additional coordinate as a first approximation. This is as far as we have gone in the present paper. Unlike GaAs-GaP studied earlier, there is no measurable fine structure in the $KNiF_3$-$KMgF_3$ system that could be compared with a model possessing more than six coordinates. It is worth outlining the next step, however, to provide a parallel comparison with the GaAs-GaP and $BaF_2$-$SrF_2$ models developed earlier.[1] Because of the crystal structure of $KNi_yMg_{1-y}F_3$, we expect that the three types of F ion do not vibrate as rigid sublattices as suggested by our three sublattice coordinates $x_2$, $x_3$, and $x_4$. For example, near an isolated Ni ion ($y\simeq 0$), the neighboring F ions should move differently than those farther away. The next step towards a more complete description is to introduce three $x_2$ coordinates $x_2^1$, $x_2^2$, and $x_2^3$. $x_2^1$ would represent an $F_2$ ion with an Mg ion on each side of it, $x_2^2$ an $F_2$ ion with an Mg ion on one side and an Ni ion on the other, and $x_2^3$ an $F_2$ ion with Ni ions on both sides. Similarly, there would be three $x_3^j$-type and three $x_4^j$-type fluorine-ion coordinates. The model would now have 12 coordinates, and therefore 11 optic modes would result. In setting up the restoring forces [e.g., row one of matrix (6)] there would be more complex probability coefficients. For example, the restoring force on a displaced potassium (ion 1) would have the three components

$$(1-y)^2k_{12}^1(x_2^1-x_1)+2y(1-y)k_{12}^2(x_2^2-x_1)+(y)^2k_{12}^3(x_2^3-x_1)\,, \qquad (16)$$

instead of the one component

$$k_{12}(x_2-x_1)\,.$$

$k_{12}^1$ represents the force on a K ion when two Mg are adjacent, and so on. As in the $BaF_2$-$SrF_2$ work,[1] it is no longer necessary to include a Grüneisen effect (Eq. 9) on the $k_{12}$ bond, since we can use a lower value for $k_{12}^3$ (pure-Ni situation) compared with $k_{12}^1$ (pure-Mg situation). The probability coefficients (shown as random probabilities here) in Eq. (16) will smoothly interpolate this K-ion force between the pure-crystal values. We have progressed from representing the F displacement around an Mg (or Ni) ion as one average value to a cluster situation with some account taken of possible real nearest-neighbor displacements. The perovskite structure has the divalent cation caged, i.e., isolated by the six nearest-neighbor fluorine ions from adjacent divalent-cation sites. This relative isolation of the ion sites on which we are performing substitutions may be the reason that the lowest level of cluster theory works so well. The Mg and Ni ions are different enough in

[18] W. J. L. Buyers and R. A. Cowley, *The Inelastic Scattering of Slow Neutrons in Solids and Liquids* (International Atomic Energy Agency, Vienna, 1968).

[19] P. Dean, Proc. Roy. Soc. (London) **A260**, 263 (1961); Proc. Phys. Soc. (London) **84**, 727 (1964).

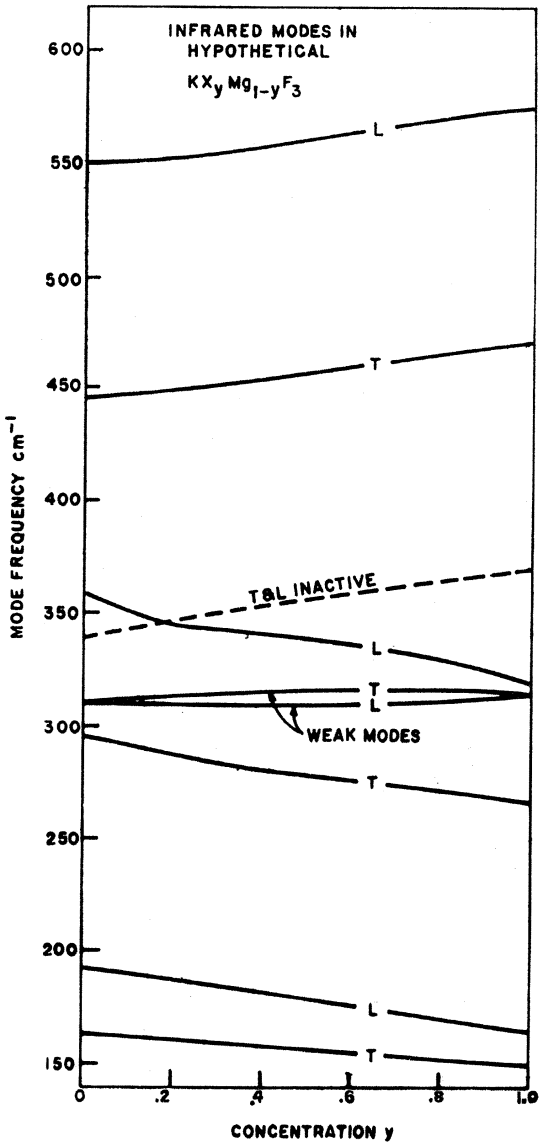


FIG. 7. Mode frequencies for a hypothetical mixed crystal of $KMgF_3$ with substitutions of Mg by an ion "$X$" with mass 35 amu but with Ni-like force constants. The 250–350-$cm^{-1}$ region now has one strong and one weak mode for all $y$.

mass and bond forces, however, that we get pronounced two-mode behavior of one of the reststrahlen bands, making a virtual-ion model inapplicable. We may use our model to show the simplification in spectra that results from Mg being replaced with an ion much lighter than Ni. To illustrate, we choose a hypothetical ion $X$ that has mass 35 (am bond u) and strengths to the F ions the same as those of Ni. For simplicity, we set the Grüneisen force-constant changes $\delta$ and $\gamma$ equal to zero. Figure 7 shows the modes that result. There are now three main reststrahlen bands at all concentrations, i.e., three TO modes with large strength. The model has four infrared-active TO modes, of course—but the fourth is insignificant in the optical spectra. This weak fourth mode has its TO and LO frequencies almost equal and causes a slight dip in the center reststrahlen band. Comparison of Fig. 7 with Fig. 6 shows that we no longer have a weak impurity mode at $y\simeq 0$ growing in strength (i.e., increasing its transverse-longitudinal splitting) and becoming a main mode at $y=1$. By reducing the "Ni-ion" mass to 35 amu, we have passed from the two-mode situation to the one-mode situation for the central reststrahlen band of these mixed fluoride perovskites. As has been discussed before, this happens when the two pure-crystal modes are fairly close in frequency.[1,3] By going to the $X$-ion of mass 35 amu, we have reduced the frequency difference between the pure crystals from 54 $cm^{-1}$ to 29 $cm^{-1}$. It is important to note, however, that we cannot predict whether a mixed-crystal system has one- or two-mode behavior from the pure-crystal spectra alone. For example, we can change the model shown in Fig. 7 to two-mode behavior by introducing small but finite values of $\delta$ and $\lambda$. This change leaves the pure-crystal modes unchanged. It is therefore apparent that we need at least the spectra of $y=0.001$ and 0.999 crystals and not $y=0$ and 1 spectra to predict mixed-crystal behavior. That is, we must know something about the impurity-mode frequencies (i.e., about $\delta$ and $\lambda$) to make even semireliable predictions about say a $y=0.50$ crystal.

In conclusion, we have developed a model that predicts the long-wavelength transverse and longitudinal optic modes in $KNi_yMg_{1-y}F_3$. A study of the model eigenvectors at $y=0.50$ shows that the central reststrahlen band is split into two separate modes primarily because Ni is much heavier than Mg. Study of a hypothetical crystal with lighter Ni mass shows that one-mode behavior is possible within the model. For this case the main modes follow virtual-ion behavior. The additional weak mode has the "Ni" vibrating *against* the Mg, giving weak dipole strength similar to certain weak modes observed experimentally in the one-mode system $Ba_ySr_{1-y}F_2$.[1]